A Monte Carlo Study of the Radiation Quality Dependence of DNA Fragmentation Spectra

Author(s): D. Alloni, A. Campa, M. Belli, G. Esposito, A. Facoetti, W. Friedland, M. Liotta, L. Mariotti, H. G. Paretzke, and A. Ottolenghi
Source: Radiation Research, 173(3):263-271.
Published By: Radiation Research Society
DOI: http://dx.doi.org/10.1667/RR1957.1
URL: http://www.bioone.org/doi/full/10.1667/RR1957.1

RADIATION RESEARCH **173**, 263–271 (2010)
0033-7587/10 $15.00

DOI: 10.1667/RR1957.1

A Monte Carlo Study of the Radiation Quality Dependence of DNA Fragmentation Spectra

D. Alloni,[a,c] A. Campa,[d,e,1] M. Belli,[d,e] G. Esposito,[d,e] A. Facoetti,[b,c] W. Friedland,[f] M. Liotta,[c] L. Mariotti,[b,c] H. G. Paretzke[f] and A. Ottolenghi[b,c]

[a] *Laboratory of Applied Nuclear Energy, Università degli studi di Pavia, Italy;* [b] *Nuclear and Theoretical Physics Department, Università degli studi di Pavia, Italy;* [c] *National Institute of Nuclear Physics (INFN), Sezione di Pavia, Italy;* [d] *Health and Technology Department, Istituto Superiore di Sanità, Roma, Italy;* [e] *National Institute of Nuclear Physics (INFN), Sezione di Roma1, Gruppo Collegato Sanità, Roma, Italy; and* [f] *Helmholtz Zentrum München, Institute of Radiation Protection, Neuherberg, Germany*

Alloni, D., Campa, A., Belli, M., Esposito, G., Facoetti, A., Friedland, W., Liotta, M., Mariotti, L., Paretzke, H. G. and Ottolenghi, A. A Monte Carlo Study of the Radiation Quality Dependence of DNA Fragmentation Spectra. *Radiat. Res.* 173, 263–271 (2010).

We simulated the irradiation of human fibroblasts with γ rays, protons and helium, carbon and iron ions at a fixed dose of 5 Gy. The simulations were performed with the biophysical Monte Carlo code PARTRAC. From the output of the code, containing in particular the genomic positions of the radiation-induced DNA double-strand breaks (DSBs), we obtained the DNA fragmentation spectra. Very small fragments, in particular those related to "complex lesions" (few tens of base pairs), are probably very important for the late cellular consequences, but their detection is not possible with the common experimental techniques. We paid special attention to the differences among the various ions in the production of these very small fragments; in particular, we compared the fragmentation spectra for ions of the same specific energy and for ions of the same LET (linear energy transfer). As found previously for iron ions, we found that the RBE (relative biological effectiveness) for DSB production was considerably higher than 1 for all high-LET radiations considered. This is at variance with the results obtainable from experimental data, and it is due to the ability to count the contribution of small fragments. It should be noted that for a given LET this RBE decreases with increasing ion charge, due mainly to the increasing mean energy of secondary electrons. A precise quantification of the DNA initial damage can be of great importance for both radiation protection, particularly in open-space long-term manned missions, and hadrontherapy.

INTRODUCTION

Energy deposition by ionizing radiation produces critical cellular lesions such as DNA double-strand breaks (DSBs) that later may lead to the manifestation of relevant biological end points. The probability of a given late cellular effect does not depend only on the number of DSBs produced; it also depends strongly on their spatial distribution. In particular, if two or several DNA damages are close, they will be repaired with less efficiency than isolated molecular damages (*1*). The sites of these damages may be geometrically close even if their genomic distance (as measured in terms of base pairs) is not small due to the chromatin conformation. The DSB distribution will be determined not only by this conformation but also by the radiation track structure at length scales down to the nanometer level, that of the DNA double helix. Therefore, it is expected that the cellular effects induced by a given dose will depend on the radiation quality. This has been found experimentally in studies of cell death, mutation induction and chromosome aberrations [see, e.g., refs. (*2–9*)]. Thus the biological effects of ionizing radiation are strongly related to the complexity of DNA damage, which affects all of the mechanisms of repair.

The determination of a relationship between radiation quality and late cellular effects needs a quantitative characterization of the early molecular (DNA) damage caused by the energy deposition events. This issue has been the focus of experimental, theoretical and simulation studies. Studies on radiation-induced DNA fragment size distributions can measure the yield of DNA DSBs and provide an estimation of the correlation between DSBs. It has been found that the DSB yield is only mildly dependent on radiation quality; on the other hand, the expected DSB correlation for high-LET radiation has been confirmed, together with an LET dependence of the DSB repair kinetics (*10–20*). On the theoretical side, both phenomenological approaches and analytical treatments have been pursued: The former tried to evaluate the DSB correlation from the analysis of fragmentation data (*21, 22*), while the latter proposed a derivation of the pattern of DSB production as

[1] Address for correspondence: Health and Technology Department, Istituto Superiore di Sanità, Viale Regina Elena 299, 00161 Roma, Italy; e-mail: campa@iss.infn.it.

determined from the interaction of the ionizing radiation with the chromatin structure (*23–25*). Simulation calculations with the Monte Carlo code PARTRAC (PARticle TRACKs) have been performed for about a decade[2] (*26–30*) to study the dependence of DNA fragmentation pattern on radiation quality. We undertook several studies in which the results of PARTRAC calculations were compared with experimental fragmentation data for different radiation qualities (*31–33*). One of our main purposes, besides the comparison with experimental data, was to visualize the very large production of very small DNA fragments after high-LET irradiation; we were particularly interested in fragments smaller than 1 kbp, which usually are not detected experimentally. Our results showed that the relative biological effectiveness (RBE) for DSB production can be significantly larger than 1. Among the cases that we have considered so far, we found the largest RBE value of about 2.4 for iron ions with LET in water of 442 keV/μm (*33*). This result is in contrast with the previously mentioned mild dependence of the DSB yield on radiation quality in the experimental data; however, these data do not include the contribution of the very small fragments to the total number of DNA fragments.

Following this line of research, in this work we make a comparison among the fragmentation patterns obtained from the PARTRAC code for a number of different radiation qualities. As emphasized in our previous work, the comparison with the experimental data, where available, has offered the opportunity to validate the code, both for the earlier version devoted only to protons and for the more recent version in which irradiations with heavy charged particles (at non-relativistic energies) are treated. Therefore, the data obtained can be reasonably trusted even without an experimental counterpart. We give special attention to the production of DNA fragments smaller than 1 kbp. These are probably very important for late cellular consequences. As such, they are relevant both (1) when the radiation damage to the cells is produced with low or very low doses, as in the situations relevant for radiation protection, and (2) when high doses are delivered, as in hadrontherapy. The case of small doses delivered by high-energy heavy particles is also relevant for radiation protection during long-term manned space missions.

It should be emphasized that the fragmentation pattern is not expected to depend only on LET, since ion beams can have the same LET but a very different track structure: A low-energy light particle can have an LET similar to that of a high-energy heavy particle, but these two particles will produce secondary electrons (delta rays) with very different energy distributions and different secondary ions. This implies that the energy deposition sites, and therefore the possible sites of the DNA damage, both direct and indirect, will have rather different spatial distributions. For irradiation with high-energy ions, we expect, in particular, a production of DSBs at large distances from the primary track. On the other hand, ions with similar specific energies (i.e., kinetic energy per nucleon) but different charges may have similar distributions for the energy of the secondary electrons, but the different LETs give rise to different fragmentation patterns. This is confirmed by our results. In fact, we have simulated, with the PARTRAC code, the irradiation of human fibroblasts with γ rays, protons and helium, carbon and iron ions at a fixed dose of 5 Gy; our main criterion has been to compare the fragmentation spectra induced by ions of the same specific energy or by ions of the same LET. The dose of 5 Gy used for all simulations was chosen as a very good compromise between the contrasting necessities to have a reasonably short calculation time and good statistics for the output data.

We show the simulation results for a number of different ions, at various energies, and we present the DNA fragment distributions, focusing in particular on the comparison between ions with equal specific energy and different LET and between ions with equal LET but different specific energy.

MATERIALS AND METHODS

The Biophysical Monte Carlo Code PARTRAC (PARticle TRACKs)

The PARTRAC code includes an accurate representation of the chromatin and of the physical and physico-chemical processes associated with the energy deposition by radiation. Different modules of the code simulate the various stages after the passage of an ionizing particle. Further details on the PARTRAC code can be found elsewhere (*27–29*).

Recently, the transport of ions in the physical module of the PARTRAC code, based on cross sections for interactions of protons in water (*29, 34*), has been suitably extended to reproduce the physics of any type of primary ion in the non-relativistic regime using scaling laws related to the mean free path of the primary ion and to the ion effective charge (Barkas formula). The results that have already been published concerning simulation with different ions are of interest for basic radiobiology, hadrontherapy and space radiation protection. The comparison with experimental fragmentation data provided a validation of the code[2] (*31–33*).

The complexity of the spatial energy deposition is related to the physical characteristics of the particle track structure. As an example of the ion tracks produced in this work, Fig. 1 shows three-dimensional track-structure portions in liquid water for carbon ions with an energy of 250 MeV/nucleon (LET = 13.8 keV/μm) and for iron ions of the same energy (LET = 260 keV/μm) obtained with the physical modules of the PARTRAC code; this module generates an output with the coordinates of each interaction point as well as the energy involved in each type of interaction. These pictures show particles with the same specific energy but different charge and consequently different LET. As expected, the track structure produced by the ion with higher Z, in this case iron, is more "dense" with respect to the lighter ion track with the same specific energy because the LET is directly proportional to the square of the particle

[2] D. Alloni, Radiation biophysics modelling: track structure theoretical bases and Monte Carlo simulations of DNA damage. Ph.D. Thesis, University of Pavia, Italy, 2008.

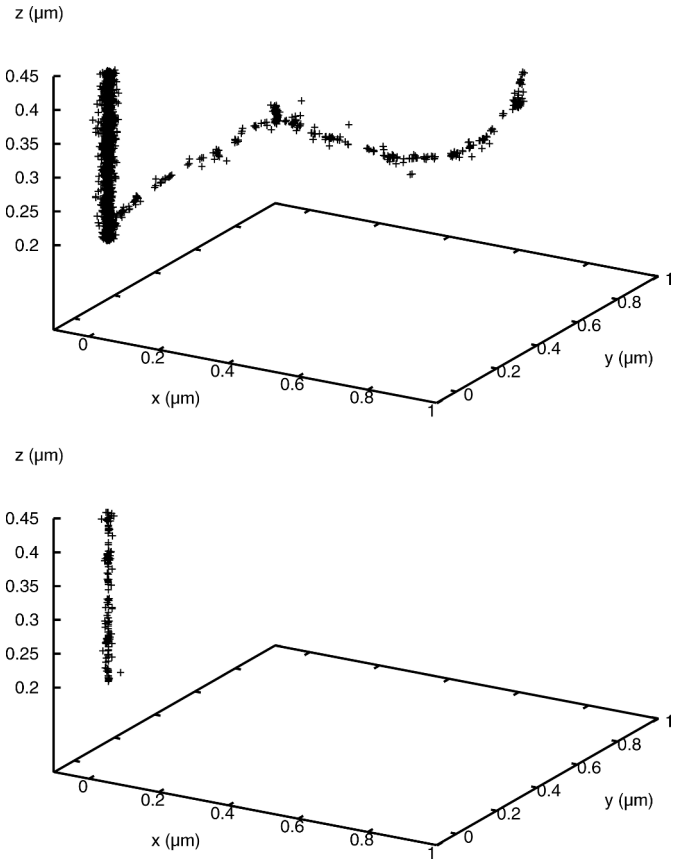

FIG. 1. Examples of track-structure segments in liquid water for iron and carbon ions with an energy of 250 MeV/nucleon as calculated with the PARTRAC code. Upper panel: 250 MeV/nucleon iron-ion track. Bottom panel: 250 MeV/nucleon carbon-ion track. The corresponding LETs in water are 260 keV/μm and 13.8 keV/μm, respectively. The considerably smaller event density around the carbon-ion track is evident. This particular iron-ion track has generated an energetic secondary electron, clearly visible in the figure.

charge. The track with the lower LET, in this case the carbon-ion track, is thus less clustered, but delta rays are energetic enough that they can travel far away with respect to the primary ion track core. This can have important consequences in terms of radiobiological damage, because energetic delta rays can reach the neighboring cells. Figure 1 shows one of these energetic delta rays generated by the iron ion.

DNA Target, Irradiation Parameters and Geometrical Simulation Setup

The DNA target model was designed to represent, on an atomic basis, the whole genome of a human fibroblast in its interphase, and it is structured in six levels of DNA organization (deoxynucleotide pair, double helix, nucleosome, chromatin fiber, chromatin fiber loops and chromosome territories). Building blocks of the model are linear chromatin fiber sticks of 150 nm and 18 kbp geometric and genomic length, respectively, with a stochastic crossed-linker arrangement of nucleosomes (Fig. 2a). About 333,000 of these fiber sticks are arranged within the 46 chromosomal territories inside a cylinder 15 μm in diameter and 5 μm high, representing the nuclear volume, forming loop structures and chromatin domains (Fig. 2b). The model is the same as the one adopted in ref. (*29*); further details are given there.

The cell nucleus model, containing the DNA surrounded by water, was irradiated from the bottom with a parallel ion beam (Fig. 2c). Table 1 summarizes the characteristics of the primary particles chosen to compare the effects of irradiation of DNA for the cases of the same LET or the same energy per nucleon (specific energy).

In the simulations, starting points, energy and directions of secondary electrons were used as input data for the electron module of the PARTRAC code; this module takes into account all the energy depositions due to the secondary electrons. The simulated yields of radiation-induced DNA strand breaks were determined by superimposing the track structure pattern on the DNA target model. It was assumed that if an inelastic energy deposition occurs in the volume occupied by the sugar-phosphate backbone or in the water shell surrounding the double helix, a single-strand break (SSB) may be produced if the energy released is larger than 5 eV (direct and quasi-direct effect, respectively). The probability of producing an SSB was assumed to increase linearly from 0 to 1 for energy depositions in the range 5–40 eV and to be equal to 1 for energy depositions larger than 40 eV. Concerning indirect effects, ionized water molecules were assumed to dissociate following the scheme $H_2O^+ + H_2O \rightarrow H_3O^+ + {}^{\bullet}OH$, whereas excited water molecules were assumed to undergo either relaxation or dissociation in the pre-chemical stage (*35*). During the chemical stage, diffusion of reactive species and their interactions with each other were considered in a step-by-step approach (*35*). An interaction between an ${}^{\bullet}OH$ and a sugar-phosphate was assumed to induce an SSB with 65% probability. Two SSBs on subsequent nucleotides in the same strand were considered as one SSB, whereas a DSB was assumed to occur when two SSBs were found on opposite strands within 10 bp. To take transfer processes into account, a conversion into a DSB was assumed for 1% of all DNA strand breaks produced by both direct and indirect effects.

Data Analysis

Fragmentation analysis was performed using the output data set of the PARTRAC effect module containing the genomic positions of DSBs. The number of double-stranded fragments, for each fragment size range was determined by calculating the distances between adjacent breaks or between a break and a chromosome end. Integral and differential DNA fragment spectra were calculated based on the DSB induction patterns and compared in particular for particles of the same specific energy and for particles of the same LET.

The analysis was performd by binning the fragments in seven different fragment size ranges: 0–30 bp, 30–1000 bp, 1–9 kbp, 9–23 kbp, 23–1000 kbp, 1000–5700 kbp and >5700 kbp. The lowest range corresponds to fragments resulting from DSBs that were previously defined operationally (*26*) as producing a "complex lesion", which was defined as a lesion determined by two or more DSBs within 30 bp. This definition was related to the likely role of such lesions in the late cellular effects. The third to sixth ranges were used in the comparisons of previous simulations with experimental data (*31–33*) in the same ranges and were kept in this work.

As already mentioned, all simulations were performed with the same dose of 5 Gy. Each point in the figures below was obtained by running the code 10 times for each radiation quality considered. We adopted two types of representations for the results: histograms showing the number of fragments in each of the seven fragment size intervals indicated previously (fragment distributions) and plots of the number of fragments with size not larger than the maximum size belonging to the ith interval for $i = 1,\ldots,7$ (cumulative fragment distributions). Error bars in the graphs are standard deviations of the results obtained in the 10 simulations.

RESULTS

Figure 3 shows the simulation results for the cumulative DNA fragment distributions induced by irradiation with different ions with the same energy of 250 MeV/nucleon at the same dose of 5 Gy. The results for the same dose of γ rays are included for comparison.

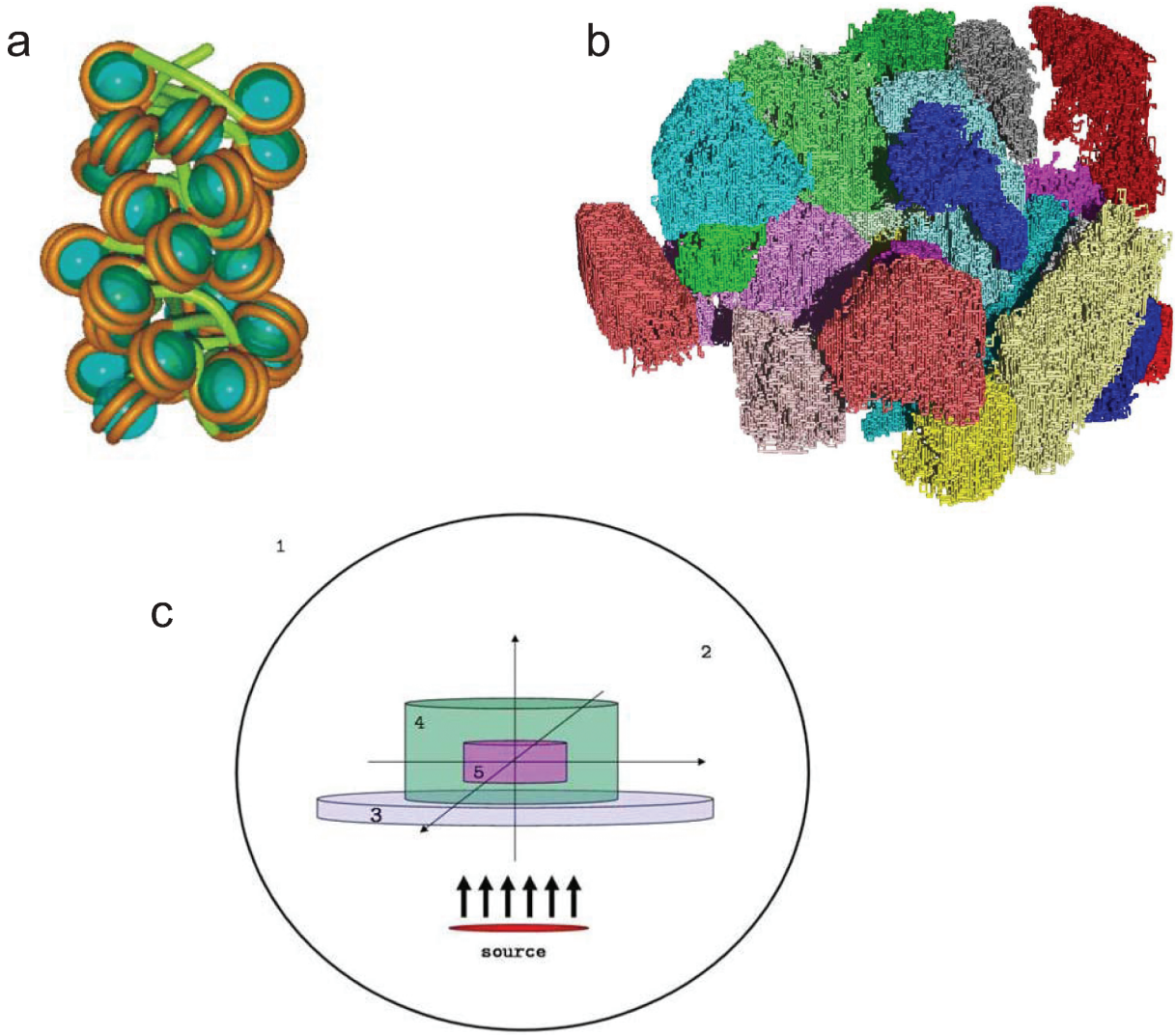

FIG. 2. Panel a: Arrangement of nucleosomes within the chromatin fiber. Histones are represented by cyan spheres, DNA attached to histones by a brown tube, and linker DNA between by a green tube. Panel b: Simulation of chromatin inside cell nucleus (corresponding to region 5 in panel c); different chromosomes are represented by different colors. Panel c: Representation of PARTRAC setup for irradiation geometry. 1, unused space; 2, void; 3, mylar; 4, cytoplasm; 5, cell nucleus. The source is represented by the red surface below the mylar; the extension and physical characteristics (i.e. primary particle spectra) can be set by the user; black arrows indicate the direction of the particle beam.

The plots indicate that the largest cumulative distribution is produced by iron ions, confirming the role of high-LET radiation in the induction of DNA fragmentation. In contrast, the fragmentation induced by the other three ions of relatively low LET do not differ considerably from that induced by γ rays. The histogram of the fragment distribution presented in Fig. 4 shows that the large fragment production due to iron ions is due mainly to the production of short fragments; for clarity, only the spectra of the iron and carbon ions are presented. In particular, large numbers of fragments are found for iron ions in the first three size ranges, i.e., 0–30 bp, 30–1000 bp and 1–9 kbp.

Comparisons between ions with the same LET but different charge and therefore different specific energy are presented in Figs. 5, 6 and 7 for LET values of 100, 201 and 442 keV/μm, respectively. As listed in Table 1, two different ions are considered for each LET. The upper panels show the histograms of the fragment distributions, while the bottom panels present the plots of the cumulative fragment distributions. In all cases, from the histograms in the upper panels we see that, for two ions with the same LET, the one with smaller specific energy produces many more small fragments, belonging to the first two size ranges. The relative difference is somewhat attenuated for the last pair of ions, those with the highest LET of 442 keV/μm (Fig. 8). In contrast, the ions with the larger energy within each pair produce more large fragments. These results can be explained as follows. The ion with the lower charge (and thus with the lower specific energy for the same LET) generates delta rays with an energy distribution shifted toward lower energies. In terms of track structure, this results in a narrower track with an enhanced production

TABLE 1
Characteristics of the Radiations used in the Simulations

Radiation (dose: 5 Gy)	Specific energy (MeV/nucleon)	LET (keV/μm)
γ rays (1)	—	~0.3
Protons (2)	250	0.4
Helium ions (3)	250	1.6
Carbon ions (4)	250	13.8
Iron ions (5)	250	260
Helium ions (6)	1.75	100
Carbon ions (7)	18.33	100
Carbon ions (8)	8.33	201
Iron ions (9)	414	201
Carbon ions (10)	2.71	442
Iron ions (11)	115	442

Notes. The entries in the first column indicate the ions considered (apart from the first row, where we also simulated ^{60}Co γ rays for comparison and RBE computation). The second and third columns give, in the rows of the ions, the specific energies and the LET in water, respectively. In the case of γ rays, we indicated an average value of the LET of the secondary electrons following the convention usually adopted. The radiations have been numbered progressively for use in reference to Fig. 8.

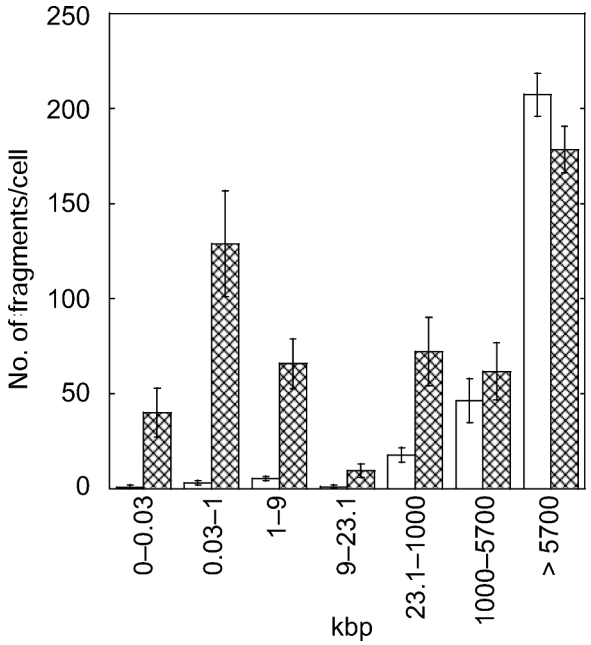

FIG. 4. Comparison between simulation results for DNA fragment spectra induced by irradiation with 250 MeV/nucleon iron ions (filled bins) and carbon ions (empty bins) with a dose of 5 Gy. Error bars are standard deviations.

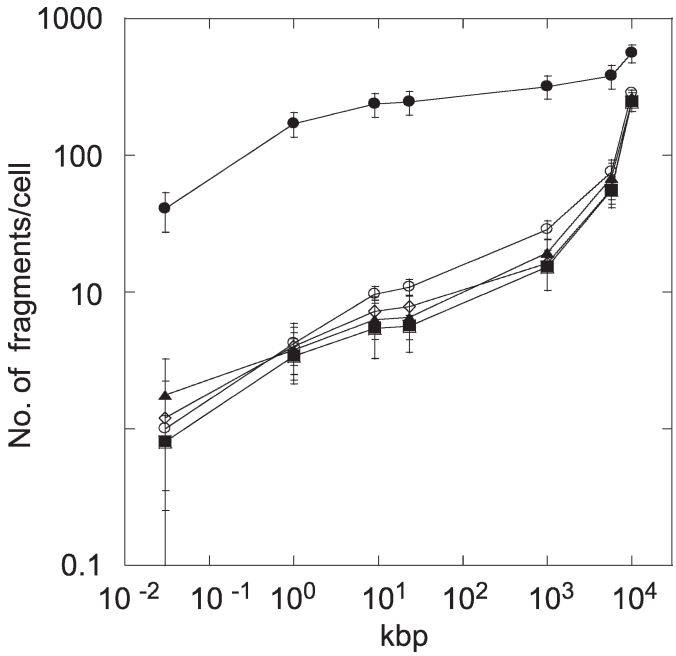

FIG. 3. PARTRAC simulation results for cumulative DNA fragment spectra induced by 5 Gy irradiation with different 250 MeV/nucleon ions: protons (0.4 keV/μm, solid squares), helium ions (1.6 keV/μm, open diamonds), carbon ions (13.8 keV/μm, open circles), iron ions (260 keV/μm, solid circles). Gamma-ray results for the same dose are shown for comparison (solid triangles). In this and in the following cumulative distributions, the abscissa denotes the largest size of the fragments represented by the corresponding point. The lines are a guide to the eye. Error bars are standard deviations and are often smaller than the symbols. In this and in the following graphs of the cumulative distributions, a log-log representation is used to obtain readable plots.

of smaller fragments. On the other hand, the more energetic delta rays generated by the ion with the higher charge are more likely to produce larger fragments. The rightmost points of the cumulative distributions shown in the bottom panels give the total number of fragments. The two effects just mentioned tend to compensate as far as this total number is concerned, but the first effect, i.e., the larger production of small fragments, appears to be more important. In Fig. 8 we present in a single histogram the total number of fragments for the 11 radiation qualities considered in this work. Each number on the abscissa refers to the progressive number given in Table 1; the left *y* axis gives the absolute values of the fragments produced by the 5-Gy irradiations, while the right *y* axis gives the RBE for fragment production, i.e., the values normalized to that of the γ rays (given the large total number of fragments produced by even a relatively low dose of 5 Gy, one can safely define this RBE also as the RBE for DSB production). The following features can be deduced from this plot: (1) As long as the LET is small (e.g. of the order of 10 keV/μm or less, as for the ions in positions 2, 3 and 4), the RBE is very close to 1; (2) for a given ion, the RBE increases with LET (helium ions in positions 3 and 6, carbon ions in positions 4, 7, 8 and 10, iron ions in positions 9, 5 and 11); (3) for a given LET, the RBE increases for decreasing charge, as shown by the three pairs in positions 6 and 7, 8 and 9, and 10 and 11, although in the last case the difference is very small relative to the error bar.

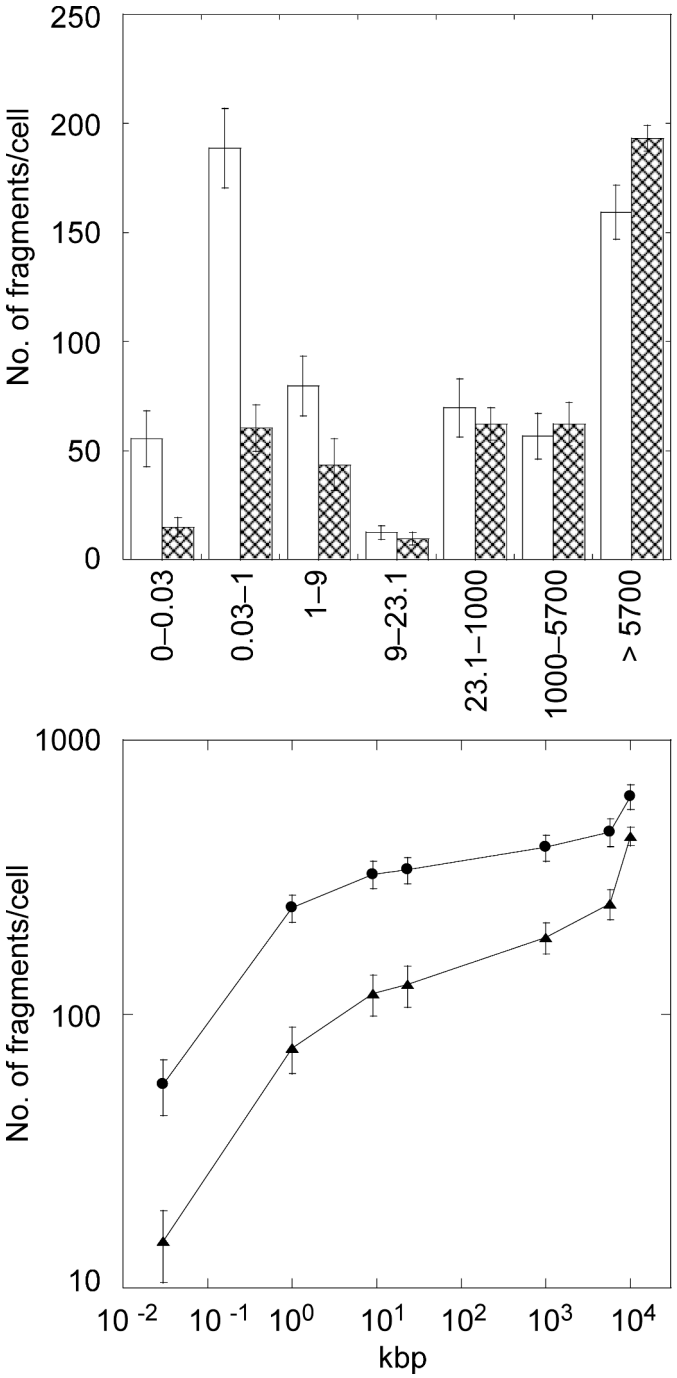

FIG. 5. Comparison between DNA fragmentation spectra induced by irradiation with 100 keV/μm helium and carbon ions with a dose of 5 Gy. Upper panel: Histogram of the fragment distribution (empty bins for helium ions and filled bins for carbon ions). Bottom panel: Cumulative fragment distributions (solid circles for helium ions and solid triangles for carbon ions); the lines are a guide to the eye. Error bars are standard deviations.

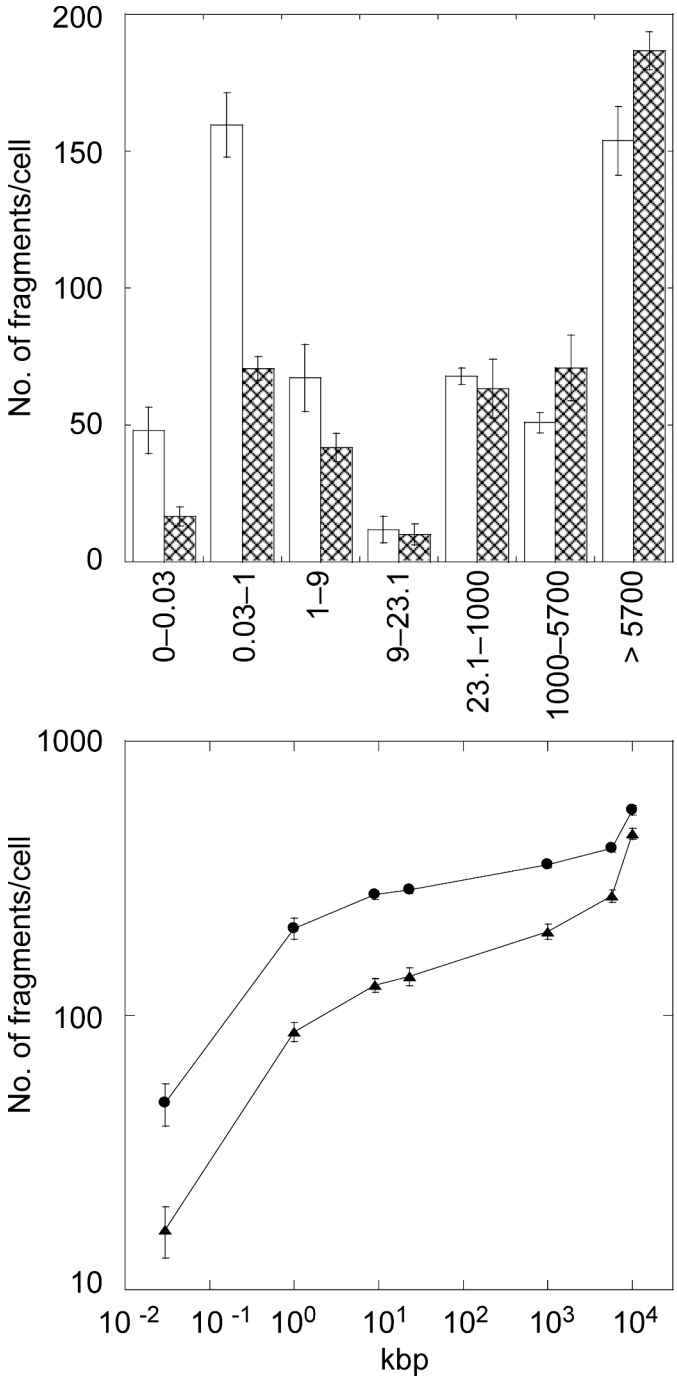

FIG. 6. Comparison between DNA fragmentation spectra induced by irradiation with 201 keV/μm carbon and iron ions with a dose of 5 Gy. Upper panel: Histogram of the fragment distribution (empty bins for carbon ions and filled bins for iron ions). Bottom panel: Cumulative fragment distributions (solid circles for carbon ions and solid triangles for iron ions); the lines are a guide to the eye. Error bars are standard deviations.

DISCUSSION AND CONCLUSIONS

Monte Carlo techniques with a realistic DNA target model describing its three-dimensional complex distribution and substructures such as the winding of DNA around histones are a necessary complement to the experimental determination of radiation-induced DNA DSBs and the consequent DNA fragmentation. This is especially valid for the study of the production of small fragments (smaller than 1 kbp). Although generally outside the possibility of experimental detection, methodologies have nevertheless been optimized that are able to count fragments of size as small as 100 bp (*11*).

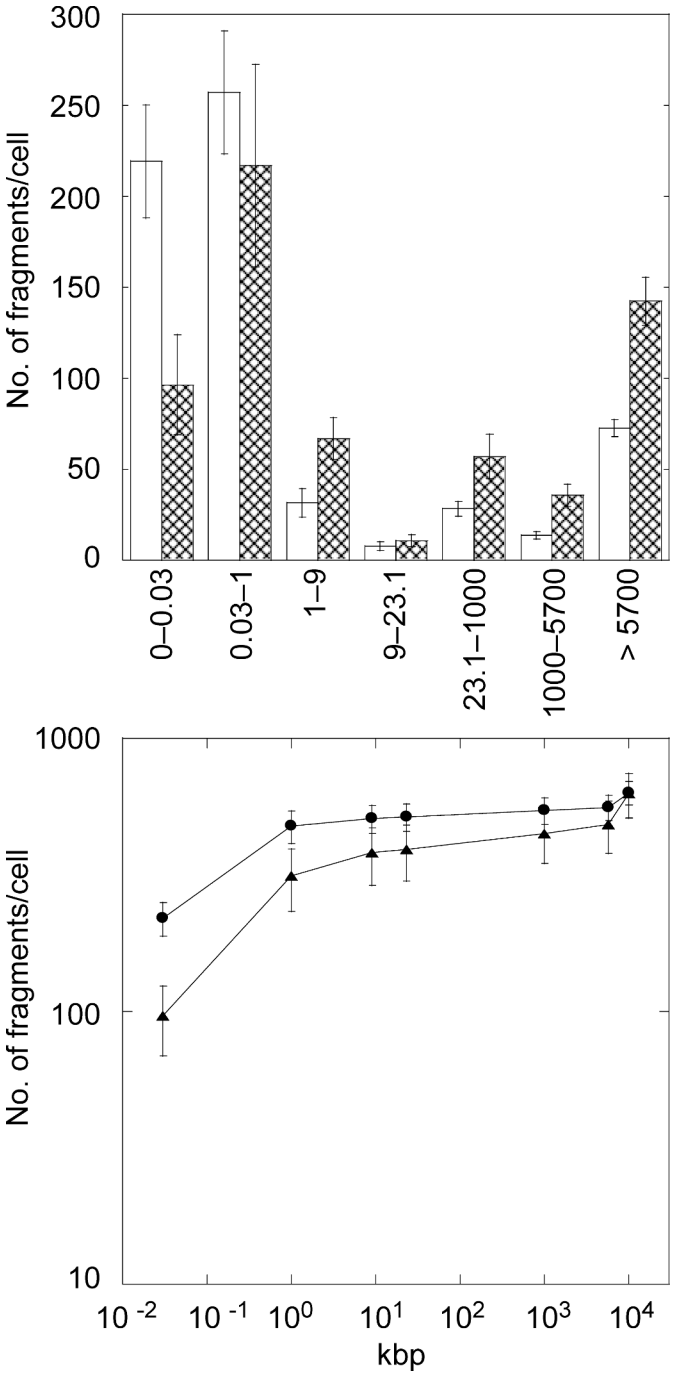

FIG. 7. Comparison between DNA fragmentation spectra induced by irradiation with 442 keV/μm carbon and iron ions with a dose of 5 Gy. Upper panel: Histogram of the fragment distribution (empty bins for carbon ions and filled bins for iron ions). Bottom panel: Cumulative fragment distributions (solid circles for carbon ions and solid triangles for iron ions); the lines are a guide to the eye. Error bars are standard deviations.

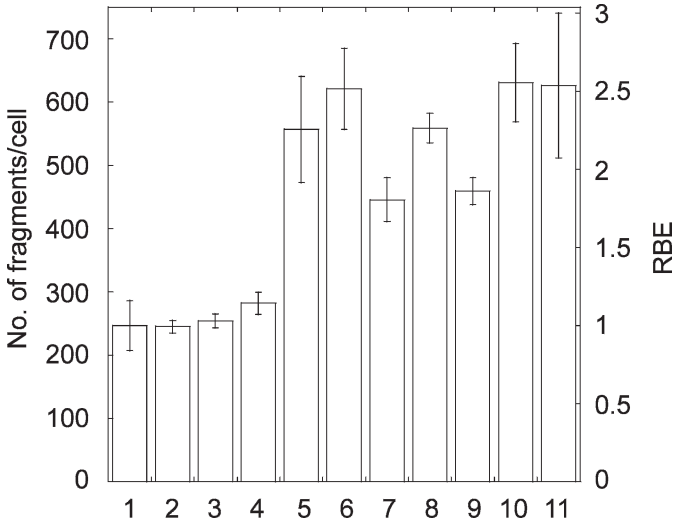

FIG. 8. Histogram of the total number of fragments produced by the 11 radiation qualities considered in this work after an irradiation with 5 Gy. The numbers in the *x* axis identify the radiation according to the progressive numbering introduced in Table 1. The scale on the left *y* axis gives the absolute fragment numbers, while the scale on the right *y* axis gives the RBE for fragment production. Error bars are standard deviations for the fragment numbers.

However, it should be taken into account that several difficulties are associated with this task. First, the problem of the background fragmentation that plagues the experimental determination of a genuinely radiation-induced fragment size distribution is particularly relevant for small fragments; this forces the use of high doses (of the order of 100 Gy) to have a reliable signal above the noise (i.e., the background fragmentation) level (*11*). However, one is generally interested in the small fragment production by single tracks, i.e., small fragments produced by correlated events; at low doses the probability of small fragments produced by different tracks is negligible. When performing irradiations with high doses, this probability becomes meaningful (although it is always smaller than for large fragments); therefore, one has to subtract the contribution from different tracks. Second, the passage from the DNA mass determination in a given size range, the experimentally measured quantity, to the number of fragments, is not without pitfalls, again especially for small fragments. One is forced to deduce this number from the ratio of the mass to a mean molecular size of the range, and generally the middle size of the range is taken. Even assuming that the middle size is the actual average size of the fragments, this does not guarantee that one obtains the correct number. These arguments should be convincing about the usefulness of the Monte Carlo evaluation of the small fragment number. In any case, apart from the ref. (*11*), we are not aware of experimental determinations of number of fragments with size smaller than 1 kbp, since the upper limit of the smallest size range is generally much larger than 1 kbp.

Obviously, the main issue with a code is its reliability in the representation of all the relevant processes that lead to the formation of DSBs. In our previous work, the validation of the PARTRAC code by comparison with available experimental data was our main concern[2] (*31–33*). The satisfactory agreement led to the conclu-

sion that the code can be reliably used to determine the fragmentation even outside the experimentally accessible range for various ions and LETs.

In Fig. 1 we have shown two typical tracks produced by a relatively low-LET carbon ion and by a high-LET iron ion of the same specific energy (radiations labeled 4 and 5 in Table 1, respectively). The two tracks have a distinctly different structure, so there are large differences in their fragment distributions (Fig. 4), cumulative distributions (Fig. 3), and RBE for fragment (or DSB) production (Fig. 8). Of particular importance for the successive damage processing and thus the late cellular effects is the difference in the first size range, that of the complex lesions, and in the second range, for fragments with sizes between 30 bp and 1 kbp. This difference is clearly related to the different cluster properties of the ionization events of the two ions. The comparisons between ions of the same LET in Figs. 5–7 and in Fig. 8 for the RBE clearly suggest that the differences in the late cellular effects caused by ions of the same LET, but different charges are rooted in the initial stages of the damage induction, with the lighter ions producing a larger amount of small fragments.

In principle, it has to be expected that the model structure is reflected in the calculated fragment distribution, in particular in the fragment size interval 10 to 40 kbp. In this respect, it is likely that the dip observed in the fragment distributions of Figs. 4 to 7 corresponding to the bin for the interval 9–23 kbp is correlated to the model structure. In fact, the 18-kbp linear chromatin fiber sticks could lead to a decrease of the number of fragments in that interval. Since the chromatin structure at that length scale is not yet known in detail, it is likely that these sticks cause an underestimation of the number of fragments in that bin and then an enhanced dip. Improved knowledge of the chromatin structure will have to be taken into account in the PARTRAC code in the future.

Carbon ions play relevant roles in hadrontherapy with ions heavier than protons (*36*), and both carbon and iron ions are important for radiation protection in space (*32, 33, 37*). Although the second issue can be considered to be important only in perspective because it is related to the problems arising in long-term manned space missions, it has been the subject of recent work (*38–40*). It links the basic research subject of the biological effects of heavy ions with a possible practical application in the future.

Here we have presented results for monoenergetic ion beams. This is the condition usually met during *in vitro* studies, where the whole cell population is traversed by ions of the same energy. There will be also a score of secondary hadrons produced by nuclear reactions, which is particularly important for heavy-ion beams. The situation is clearly different if we consider the traversal of the human body. Due to the stochastic nature of energy depositions, even an initially monoenergetic beam gradually degrades and spreads in energy with depth, and therefore the cells will be hit, beyond the secondary hadrons, by primary ions with different energies. This feature is even purposely enhanced when use is made of a spread-out Bragg peak. However, the production of very small DNA fragments has a simple additive property (unless the doses delivered are very high), since most of these fragments, which are the result of energy depositions within the nanometer scale, are due to correlated events from the same track. The additive property will not extend to the late cellular effects, since there is no evidence that the repair capability, or more generally the damage processing, depends only on the damage clustering at the smallest scale. This implies that a precise and detailed determination of DSB distribution is only the first step in the construction of the relationship between track structure and cellular effects. The other, more difficult, step would be a better knowledge of the relationship between the DSB distribution and the kinetics of damage processing. However, the quantification of the initial damage induction is necessary to understand the dependence of the late effects on radiation quality. We believe that the PARTRAC Monte Carlo code offers one of the best tools for such investigations.

ACKNOWLEDGMENTS

This work was partially supported by EU (“RISC-RAD” project, Contract no. FI6R-CT 2003- 508842, and “NOTE” project, Contract no. FI6R-036465) and ASI (Italian Space Agency, “Mo-Ma/Count” project).

Received: August 4, 2009; accepted: November 3, 2009; published online: January 4, 2010

REFERENCES

1. D. T. Goodhead, Initial events in the cellular effects of ionising radiations: clustered damage in DNA. *Int. J. Radiat. Biol.* **65**, 7–17 (1994).
2. M. Suzuki, M. Watanabe, T. Kanai, Y. Kase, F. Yatagai, T. Kato and S. Matsubara, LET dependence of cell death, mutation induction and chromatin damage in human cells irradiated with accelerated carbon ions. *Adv. Space Res.* **18**, 127–136 (1996).
3. M. Belli, F. Cera, R. Cherubini, M. Dalla Vecchia, A. M. I. Haque, F. Ianzini, G. Moschini, O. Sapora, G. Simone and P. Tiveron, RBE-LET relationships for cell inactivation and mutation induced by low energy protons in V79 cells: further results at the LNL facility. *Int. J. Radiat. Biol.* **74**, 501–509 (1998).
4. R. M. Anderson, S. J. Marsden, E. G. Wright, M. A. Kadhim, D. T. Goodhead and C. S. Griffin, Complex chromosome aberrations in peripheral blood lymphocytes as a potential biomarker of exposure to high-LET α-particles. *Int. J. Radiat. Biol.* **76**, 31–42 (2000).
5. F. Belloni, D. Bettega, P. Calzolari, R. Cherubini, P. Massariello and L. Tallone, Inactivation cross sections for mammalian cells exposed to charged particles: A phenomenological approach. *Radiat. Prot. Dosimetry* **99**, 199–202 (2002).

6. K. George, M. Durante, H. Wu, V. Willingham and F. A. Cucinotta, *In vivo* and *in vitro* measurements of complex-type chromosomal exchanges induced by heavy ions. *Adv. Space Res.* **31**, 1525–1535 (2003).
7. M. Durante, K. George, G. Gialanella, G. Grossi, C. La Tessa, L. Manti, J. Miller, M. Pugliese, P. Scampoli and F. A. Cucinotta, Cytogenetic effects of high-energy iron ions: dependence on shielding thickness and material. *Radiat. Res.* **164**, 571–576 (2005).
8. R. Lee, E. Nasonova and S. Ritter, Chromosome aberrations yields and apoptosis in human lymphocites irradiated with Fe-ions of differing LET. *Adv. Space Res.* **35**, 268–275 (2005).
9. D. Bettega, P. Calzolari, L. Doneda, M. Durante and L. Tallone, Early and delayed reproductive death in human cells exposed to high energy iron ion beams. *Adv. Space Res.* **35**, 280–285 (2005).
10. M. Löbrich, P. K. Cooper and B. Rydberg, Non-random distribution of DNA double-strand breaks induced by particle irradiation. *Int. J. Radiat. Biol.* **70**, 493–503 (1996).
11. B. Rydberg, Clusters of DNA damage induced by ionizing radiation: Formation of short DNA fragments. II. Experimental detection. *Radiat. Res.* **145**, 200–209 (1996).
12. H. C. Newman, K. M. Prise, M. Folkard and B. D. Michael, DNA double-strand break distributions in X-ray and α-particle irradiated V79 cells: evidence for non-random breakage. *Int. J. Radiat. Biol.* **71**, 347–363 (1997).
13. M. Löbrich, P. K. Cooper and B. Rydberg, Joining of correct and incorrect DNA ends at double-strand breaks produced by high-linear energy transfer radiation in human fibroblasts. *Radiat. Res.* **150**, 619–626 (1998).
14. K. M. Prise, G. Ahnström, M. Belli, J. Carlsson, D. Frankenberg, J. Kiefer, M. Löbrich, B. D. Michael, J. Nygren and B. Stenerlöw, A review of dsb induction data for varying quality radiation. *Int. J. Radiat. Biol.* **74**, 173–184 (1998).
15. B. Rydberg, W. R. Holley, I. S. Mian and A. Chatterjee, Chromatin conformation in living cells: support for a zig-zag model of the 30 nanometer chromatin fiber. *J. Mol. Biol.* **284**, 71–84 (1998).
16. D. Frankenberg, H. J. Brede, U. J. Schrewe, C. Steinmetz, M. Frankenberg-Schwager, G. Kasten and E. Pralle, Induction of DNA double-strand breaks by ^{1}H and ^{4}He ions in primary human skin fibroblasts in the LET range of 8 to 124 keV μm^{-1}. *Radiat. Res.* **151**, 540–549 (1999).
17. E. Höglund, E. Blomquist, J. Carlsson and B. Stenerlöw, DNA damage induced by radiation of different linear energy transfer: initial fragmentation. *Int. J. Radiat. Biol.* **76**, 539–547 (2000).
18. M. Belli, R. Cherubini, M. Dalla Vecchia, V. Dini, G. Esposito, G. Moschini, O. Sapora, G. Simone and M. A. Tabocchini, DNA fragmentation in V79 cells irradiated with light ions as measured by PFGE. I. Experimental results. *Int. J. Radiat. Biol.* **78**, 475–482 (2002).
19. B. Stenerlöw and E. Höglund, Rejoining of double-stranded DNA-fragments studied in different size-intervals. *Int. J. Radiat. Biol.* **78**, 1–7 (2002).
20. E. Pastwa, R. D. Neumann, K. Mezhevaya and T. A. Winters, Repair of radiation-induced DNA double-strand breaks is dependent upon radiation quality and the structural complexity of double-strand breaks. *Radiat. Res.* **159**, 251–261 (2003).
21. A. Campa, G. Esposito, M. Belli, G. Simone and M. A. Tabocchini, DNA fragmentation in V79 cells irradiated with light ions as measured by pulsed-field gel electrophoresis. II. Simulation with a generalized broken stick model. *Int. J. Radiat. Biol.* **80**, 229–238 (2004).
22. M. Pinto, K. M. Prise and B. D. Michael, A Monte Carlo model of DNA double-strand break clustering and rejoining kinetics for the analysis of pulsed-field gel electrophoresis data. *Radiat. Res.* **162**, 453–463 (2004).
23. W. R. Holley and A. Chatterjee, Clusters of DNA damage induced by ionizing radiation: formation of short DNA fragments. I. Theoretical modeling. *Radiat. Res.* **145**, 188–199 (1996).
24. R. K. Sachs, A. L. Ponomarev, P. J. Hahnfeldt and L. R. Hlatky, Locations of radiation-produced DNA double strand breaks along chromosomes: a stochastic cluster process formalism. *Math. Biosci.* **159**, 165–187 (1999).
25. A. L. Ponomarev and R. K. Sachs, Radiation breakage of DNA: a model based on random-walk chromatin structure. *J. Math. Biol.* **43**, 356–376 (2001).
26. A. Ottolenghi, M. Merzagora, L. Tallone, M. Durante, H. G. Paretzke and W. E. Wilson, The quality of DNA double-strand breaks: a Monte Carlo simulation of the end-structure of strand breaks produced by protons and alpha particles, *Radiat. Environ. Biophys.* **34**, 239–244 (1995).
27. W. Friedland, P. Jacob, H. G. Paretzke and J. Stork, Monte Carlo simulation of the production of short DNA fragments by low-linear energy transfer radiation using higher-order DNA models. *Radiat. Res.* **150**, 170–182 (1998).
28. W. Friedland, P. Jacob, H. G. Paretzke, M. Merzagora and A. Ottolenghi, Simulation of DNA fragment distributions after irradiation with photons. *Radiat. Environ. Biophys.* **38**, 39–47 (1999).
29. W. Friedland, P. Jacob, P. Bernhardt, H. G. Paretzke and M. Dingfelder, Simulation of DNA damage after proton irradiation. *Radiat. Res.* **159**, 401–410 (2003).
30. W. Friedland, P. Jacob, H. G. Paretzke, A. Ottolenghi, F. Ballarini and M. Liotta, Simulation of light ion induced DNA damage patterns. *Radiat. Prot. Dosimetry* **122**, 116–120 (2006).
31. A. Campa, F. Ballarini, M. Belli, R. Cherubini, V. Dini, G. Esposito, W. Friedland, S. Gerardi, S. Molinelli and M. A. Tabocchini, DNA DSB induced in human cells by charged particles and gamma rays: experimental results and theoretical approaches. *Int. J. Radiat. Biol.* **81**, 841–854 (2005).
32. D. Alloni, F. Ballarini, M. Belli, A. Campa, G. Esposito, W. Friedland, M. Liotta, A. Ottolenghi and H. G. Paretzke, Modeling of DNA fragmentation induced in human fibroblasts by ^{56}Fe ions. *Adv. Space Res.* **40**, 1401–1407 (2007).
33. A. Campa, D. Alloni, F. Antonelli, F. Ballarini, M. Belli, V. Dini, G. Esposito, A. Facoetti, W. Friedland and M. A. Tabocchini, DNA fragmentation induced in human fibroblasts by ^{56}Fe ions: experimental data and Monte Carlo simulations. *Radiat. Res.* **171**, 438–445 (2009).
34. M. Dingfelder, M. Inokuti and H. G. Paretzke, Inelastic-collision cross sections of liquid water for interactions of energetic protons. *Radiat. Phys. Chem.* **59**, 255–275 (2000).
35. F. Ballarini, M. Biaggi, M. Merzagora, A. Ottolenghi, M. Dingfelder, W. Friedland, P. Jacob and H. G. Paretzke, Stochastic aspects and uncertainties in the prechemical and chemical stages of electron tracks in liquid water: a quantitative analysis based on Monte Carlo simulations. *Radiat. Environ. Biophys.* **39**, 179–188 (2000).
36. H. Tsujii, T. Kamada, M. Baba, H. Tsuji, H. Kato, S. Kato, S. Yamada, S. Yasuda, T. Yanagi and J. Mizoe, Clinical advantages of carbon-ion radiotherapy. *New J. Phys.* **10**, 075009 (1–16) (2008).
37. F. Ballarini, D. Alloni, A. Facoetti and A. Ottolenghi, Heavy-ion effects: from track structure to DNA and chromosome damage. *New J. Phys.* **10**, 075008 (1–17) (2008).
38. M. Durante, Biological dosimetry in astronauts. *Riv. Nuovo Cimento* **19**, 1–44 (1996).
39. M. Durante, K. George, H. Wu and F. Cucinotta, Karyotypes of human lymphocytes exposed to high-energy iron ions. *Radiat. Res.* **158**, 581–590 (2002).
40. M. Durante, G. Snigiryova, E. Akaeva, A. Bogomazova, S. Druzhinin, B. Fedorenko, O. Greco, N. Novitskaya, A. Rubanovich and G. Obe, Chromosome aberration dosimetry in cosmonauts after single or multiple space flights *Cytogenet. Genome Res.* **103**, 40–46 (2003).